IEEE Access
Multidisciplinary | Rapid Review | Open Access Journal

Received March 1, 2020, accepted March 22, 2020, date of publication March 30, 2020, date of current version April 17, 2020.

Digital Object Identifier 10.1109/ACCESS.2020.2984006

Differential Fiber Optic Gyroscope Driven by Two Broadband Sources of Different Wavelengths

YUANHONG YANG[1], SHUAI LI[1], FULING YANG[1], AND WEI JIN[2]
[1]School of Instrumentation and Optoelectronic Engineering, Beihang University, Beijing 100191, China
[2]Department of Electrical Engineering, The Hong Kong Polytechnic University, Hong Kong

Corresponding author: Yuanhong Yang (yhyang@buaa.edu.cn)

This work was supported in part by the National Natural Science Foundation of China (NSFC) under Grant U1637106 and Grant 61227902, in part by the National Key Research and Development Program of China under Grant 2018YFC1503703, and in part by the Program for Innovative Research Team in University under Grant IRT 1203.

ABSTRACT We propose a differential fiber optic gyroscope driven by two broadband light sources with different wavelengths. Preliminary experiments demonstrate that both bias drift and angle random walk can be reduced considerably due to common-mode error cancellation. Theoretical analysis shows that the effect of transient temperature could be eliminated by optimizing the dispersion of the fiber coil and/or by introducing a dispersion compensation factor before taking the differential operation. Experiments with a fiber coil with weak wavelength-dependent dispersion coefficient show that significant reduction of bias drift due to transient temperature can be achieved with a proper dispersion compensation factor.

INDEX TERMS Dual light sources, gyroscopes, optical fiber sensors.

I. INTRODUCTION

After more than forty years of research and development, interferometric fiber optic gyroscopes (FOGs) have achieved remarkably good performance in terms of short-term noise (i.e., angle random walk or ARW) and long-term bias drift. It is regarded as the most promising candidate for the ''ultimate-performance'' gyroscopes [1]–[4]. Several sources of noise, including coherent backscatters, shot and thermal noises in photoreceiver are largely overcome by using high power broadband sources, leaving the excess source relative intensity noise (RIN) as the dominant noise contributor [5]. Techniques such as electronic RIN subtraction [6], optical RIN subtraction [7], using an interferometric filter [8] and application of the Wiener filter [9] have been developed to reduce the RIN and good performance has been achieved. The bias drift is largely caused by time-varying temperature gradient along the fiber [10], [11], which can be reduced effectively by symmetric fiber-winding [12], proper mechanical packaging [13], adopting a heating insulation cavity [14], and other methods [15], [16]. However, the bias stability of current FOGs is still limited by the effect of transient temperature and further reduction or elimination of errors due to this effect, without using sophisticated precision temperature control, might be one of the final challenges for high-performance FOGs.

We have previously demonstrated a low noise closed-loop FOG driven simultaneously by two broadband sources and the noise of that FOG is reduced considerably due to the super broad spectral width of the combined source. However, it has no advantage in the reduction of bias drift due to transient temperature. In this letter, we report a differential FOG (DFOG) which is composed of two equivalent interferometric FOGs sharing one Sagnac interferometer assembly (SIA) and driven by two broadband sources with different wavelengths. This DFOG has good common-mode error rejection capability and may achieve low bias drift due to transient temperature by specially designing operational parameters and data processing methods. In section II, the structure of the DFOG is presented and the operation principle is explained. Theoretical formulations and optimal operation conditions are derived. In section III, test results of the DFOG at ambient temperature are presented. In section IV, the bias drift induced by transient temperature is investigated. By introducing a dispersion compensation factor, the bias drift of the DFOG with a fiber coil made of weak wavelength-dependent dispersion fiber can be largely reduced.

The associate editor coordinating the review of this manuscript and approving it for publication was Muguang Wang.

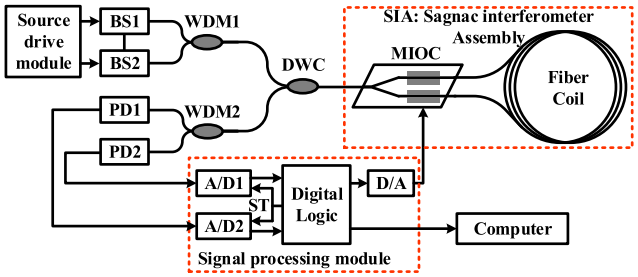

FIGURE 1. Schematic of the DFOG. BS: Broadband Sources, WDM: Wavelength Division Multiplexer, DWC: Dual-Window Fiber Coupler, MIOC: Multifunctional Integrated Optical Circuit, SIA: Sagnac Interferometer Assembly, A/D: Analog to Digital Converter, ST: Synchronous Trigger, D/A: Digital to Analog Converter.

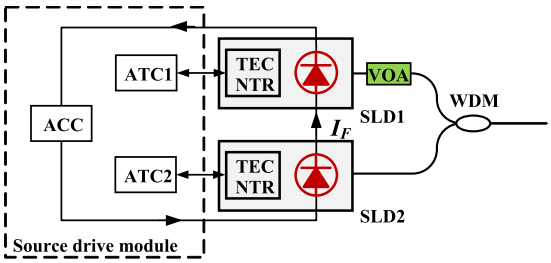

FIGURE 2. Schematic of source driver module. ACC: Automatic Current Control Circuit, ATC: Automatic Temperature Control Circuit, TEC: Thermoelectric Cooler, NTR: Negative Temperature Resistance, SLD: Superluminescent Diode, VOA: Variable Optical Attenuator, I_F: Driving Current.

II. BASIC PRINCIPLE OF DFOG

The schematic of the proposed DFOG is shown in Fig. 1. Light outputs from two broadband sources (BS1 and BS2) with respective mean wavelengths of λ_1 and λ_2 are combined with a wavelength division multiplexer (WDM1). A dual-window fiber coupler (DWC) that operates simultaneously at λ_1 and λ_2 leads the combined light beam into a Sagnac interferometer assembly (SIA). The same DWC also leads the output from the SIA to a second wavelength division multiplexer (WDM2) at which the two source wavelengths (i.e., at λ_1 and λ_2) are separated and detected by two photodetectors (PD1 and PD2), respectively. The SIA is composed of a custom made multifunctional integrated optical circuit (MIOC) and a fiber coil. The MIOC was specially fabricated and can operate at both λ_1 and λ_2 [17]. The cut-off wavelength of the fibers used in the optical circuit and the fiber coil is short enough, which guarantees single-mode propagation at λ_1 and λ_2 simultaneously. The system can be regarded as two equivalent FOGs, namely FOG1 and FOG2 with operating wavelength λ_1 and λ_2 respectively, sharing the same SIA. The output of DFOG is the difference of the output signals from the two equivalent FOGs, and errors common to the two FOGs are then minimized due to common-mode error cancellation.

Figure 2 shows the source driver module, which has been described in [17]. The temperatures of the two SLD chips are controlled independently by an automatic temperature control circuit (ATC) with integrated thermoelectric cooler (TEC) and negative temperature resistance (NTR). The two SLDs are connected in serial and are driven by an automatic current control (ACC) circuit with the same driving current I_F. Under the same driving current, the output power levels of the two SLDs are typically not equal and hence a variable optical attenuator (VOA) is inserted in the output port of the SLD with a relatively larger power level to balance their operational power levels. This helps to keep the fluctuations due to driving current in the two SLDs consistent.

An all-digital open-loop signal processing module was designed, as shown in Fig. 1. The square wave signal is generated in the digital logic with D/A converter and added on MIOC, the output from PD1 and PD2 are converted to digital value directly by the two A/D converters, which are synchronized under one synchronous trigger (ST). The digital output v_j from each of the equivalent FOGs may be expressed as [18]:

$$\begin{aligned} v_j &= K_j \sin(\varphi_j) = 2P_jG_j \sin(\varphi_{bj}) \sin(\varphi_j), \\ K_j &= 2P_jG_j \sin(\varphi_{bj}), \end{aligned} \tag{1}$$

where $j = 1, 2$, represent the two equivalent FOGs driven by λ_1 and λ_2 sources respectively. P_j is light power on the photodetector, G_j is the gain coefficient of the digital signal processing module, φ_{bj} is the phase modulation depth and K_j is a compositive coefficient. φ_j is the total phase of the j-th equivalent FOG, which can be expressed as:

$$\begin{aligned} \varphi_j &= K_{Sj} \cdot \Omega + \varphi_{ej} + \varepsilon_j, \\ K_{Sj} &= \frac{2\pi LD}{\lambda_j c}, \end{aligned} \tag{2}$$

where K_{Sj} is the Sagnac factor with operational wavelength λ_j, Ω is input rotation rate, φ_{ej} is error phase drift and ε_j is noise, L and D are the length and diameter of the fiber coil respectively, and c is the speed of light in vacuum.

The output of the DFOG is the phase difference φ_D between the two equivalent FOGs and can be described as:

$$\begin{aligned} \varphi_D &= \varphi_1 - \varphi_2 = K_{SD} \cdot \Omega + \Delta\varphi_e + \varepsilon_D, \\ K_{SD} &= \frac{2\pi LD}{c} \cdot \frac{\lambda_2 - \lambda_1}{\lambda_1\lambda_2}, \\ \Delta\varphi_e &= \varphi_{e1} - \varphi_{e2}, \end{aligned} \tag{3}$$

where K_{SD} is the Sagnac factor of DFOG and reduced with a ratio of $(\lambda_2\text{-}\lambda_1)/\lambda_j$. $\Delta\varphi_e$ is the residual phase error and ε_D is the noise of DFOG. The noises suppressed in ε_D contains two main parts, one is the common-mode noise due to the polarization non-reciprocity, coherent back reflection, backscatter noises, and, time transience-related nonreciprocal effects, etc. in the SIA. The other is the random noise associated with relative intensity noise (RIN).

With suitable operational parameters, we can make $K_1 = K_2$. For evaluating noise and drift, we may also assume that φ_1 and φ_2 are small and use the approximation of sin $\varphi_j \approx \varphi_j$. The difference between the outputs of FOG1 and

FOG2 can be taken directly as the output v_D of the DFOG:

$$\begin{aligned} v_1 &= K_1\varphi_1 = 2P_1G_1\sin(\varphi_{b1})\,\varphi_1, \\ v_2 &= K_2\varphi_2 = 2P_2G_2\sin(\varphi_{b2})\,\varphi_2, \\ v_D &= v_1 - v_2 = K_1\varphi_1 - K_2\varphi_2 = K_D\cdot(\varphi_1-\varphi_2), \end{aligned} \quad (4)$$

where K_D is a compositive coefficient of the DFOG, and $K_1 = K_2 = K_D$. And the output rotation rate of DFOG can be calculated based on (3) and (4), as:

$$\Omega = v_D/(K_D\cdot K_{SD}). \quad (5)$$

In the DFOG, the two equivalent FOGs share the same SIA. Hence the phase errors φ_{ej} produced in the SIA, if they are wavelength-independent to some degree, may be reduced or even eliminated by the differential processing as stated in (3).

A particular type of error that may benefit from differential processing is the effect of temperature transience (Shupe effect). As first demonstrated by Shupe [10], when temperature T varies as a function of both time t and position l along the fiber, the induced phase error φ_{ej} may be expressed as:

$$\varphi_{ej} = \frac{2\pi n_{cj}}{\lambda_j c}\left(\frac{dn_{cj}}{dT} + \alpha n_{cj}\right)\int_0^L [T(t,l) - T(0,l)](2l-L)dl, \quad (6)$$

where n_{cj} is the refractive index of the fiber core at operational wavelength λ_j and α is the thermal expansion coefficient of silica. To simplify the equation, we may define a wavelength-dependent dispersion coefficient D_j and a wavelength-independent coefficient F in (6):

$$\begin{aligned} D_j &= n_{cj}\left(\frac{dn_{cj}}{dT} + \alpha n_{cj}\right), \\ F &= \frac{2\pi}{c}\int_0^L [T(t,l) - T(0,l)](2l-L)dl. \end{aligned} \quad (7)$$

The phase error $\Delta\varphi_e$ due to Shupe effect may be rewritten as:

$$\Delta\varphi_e = F\cdot\left(\frac{D_1}{\lambda_1} - \frac{D_2}{\lambda_2}\right). \quad (8)$$

We can see that the $\Delta\varphi_e$ becomes zero if the D_1/λ_1 equals to D_2/λ_2. Although this condition can be hardly satisfied with the current fiber coils since the dispersion of the fibers used is typically very weak. However, it points out a direction for possible elimination of temperature transience by fabricating a fiber with special dispersion properties or developing special techniques to partially overcome the problem. Besides, there are other errors such as coherent back reflection and backscatter noises that are common to the two equivalent FOGs (since they share the same current driver and one SIA), which may be reduced by use of the differential processing.

TABLE 1. The main components and their parameters.

Components	Main parameters
BS1	SLD: λ1=1304.1nm, Δλ1=45.7nm, Power>3.8mW, PER=0.53dB
BS2	SLD: λ2=1559.6nm, Δλ2=64.8nm, Power>3.1mW,.PER=0.56dB
VOA	Attenuation Range: 0 to 40dB Resolution: 0.1dB
WDM1&2	1310/1550 CWDM, IL<0.5dB, PDL<0.03dB
DWC	1310/1550±40nm, IL<0.5dB, PDL<0.06dB
MIOC	V_π: 2.70V@1310nm, 3.37V@1550nm, IL: ~3.40dB
PD1&2	InGaAs PIN-FET, 1100nm to 1650nm
Fiber Coil	Panda PM fiber, ~3km, Coil diameter: 170mm

SLD: Superluminescent Diodes, PER: Polarization Extinction Ratio, IL: Insertion Loss, PDL: Polarization Dependent Loss, PM: Polarization Maintaining, V_π: Half Wave Voltage.

III. NOISE AND BIAS DRIFT OF DFOG

An experimental DFOG was built based on the structure shown in Fig. 1. The main components and their parameters are listed in Table 1. Two high power and low polarization SLDs with different wavelengths from Wuhan Yingfeihua Technology Corporation Limited were selected and driven by the ACC circuit with the same driving current. The output power of SLD1 ($\lambda1 = 1304.1$ nm) and SLD2 ($\lambda2 = 1559.6$ nm) are about 3.8 and 3.1 mW when the driving current is $I_F \approx 162$ mA, and the polarization extinction ratios of the SLDs are weak and about 0.53 and 0.56 dB for SLD1 and SLD2 respectively. A variable optical attenuator (Opto-Link Corporation Limited Manual VOA) was inserted in the output port of SLD1 to balance the operational power of SLDs. The fiber coil has a diameter of ~170 mm and is made of ~3-km-long Panda polarization maintaining (PM) fiber. In the all-digital open-loop signal processing module, the amplitude of the square wave is designed optimally to achieve bias modulation near $\pi/2$ radians in each of the equivalent IFOGs. The outputs of the two equivalent FOGs are acquired synchronously and demodulated separately with the digital logic module and the differential processing is carried out on the computer.

To satisfy (4), we set and adjusted the operational parameters of DFOG step by step. First, the light power P_j on the photodetectors of the equivalent FOG1 and FOG2 were set approximately equal by adjusting the variable optical attenuator at the output of SLD1. Then, the scale factors of the two equivalent FOGs were measured by applying small rotation within $\sim \pm1$ °/s and the P_j was adjusted again to let K_1 be closer to K_2. This parameter adjustment process was repeated until K_1 is equal to K_2. The digital gain coefficient G_j in (1) was finely adjusted finally based on the measured scale factors to make $K_1 = K_2 = K_D$ exactly in the digital logic circuit. At last, the rotation response of the equivalent FOGs and DFOG were tested over a larger rotation range of ±50 °/s. During experiment, fine rotation step of 0.5 °/s was applied

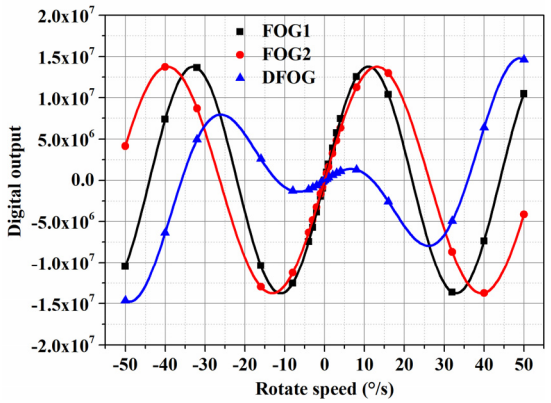

FIGURE 3. The measured and calculated rotation response of the equivalent FOGs and DFOG. The solid-line curves are calculated results and the dots are measured results for different rotation rates applied.

TABLE 2. *SFs* and K_{Sj} parameters of FOGs.

	SF_j (°/s)$^{-1}$	K_{Sj} (s)
FOG1	1967056	8.19064
FOG2	1644806	6.84882
DFOG	322250	1.34182

within ±2 °/s, and other rotation rates applied were ±3, ±4, ±8, ±16, ±32, ±40, and ±50 °/s. The fine tuning was carried out further to guarantee that (4) is satisfied strictly. Then, the rotation response may be obtained based on (1)-(4) by use of the parameters listed in Table 1 and the measured value of K_D. The relations between the digital outputs and the rotation rates are summarized as follows:

$$v_1 = K_1 \sin(\frac{2\pi LD}{\lambda_1 c} \cdot \Omega),$$
$$v_2 = K_2 \sin(\frac{2\pi LD}{\lambda_2 c} \cdot \Omega),$$
$$v_D = K_D \left[\sin(\frac{2\pi LD}{\lambda_1 c} \cdot \Omega) - \sin(\frac{2\pi LD}{\lambda_2 c} \cdot \Omega)\right]. \quad (9)$$

Figure 3 shows the measured results and the calculated response curves. When the measurement data all lay exactly in the calculated curves, indicating that (4) is satisfied and the value of the compositive coefficient is determined to be $K_1 = K_2 = K_D = 240159\ (^\circ)^{-1}$, The Scale Factors (*SFs*) for small rotation rates and the values of K_{Sj} of the equivalent FOGs and the DFOG are listed in Table 2.

The zero biases of the equivalent FOGs and DFOG were tested at ambient temperature. The measurement data v_1 and v_2 of the equivalent FOGs are converted to rotation rates directly by using values of SF_1 and SF_2 listed in Table 2 respectively, while the output data of DFOG is the difference between v_1 and v_2, and the differential value was converted to rotation rate by using the *SF* of the DFOG in Table 2. The measured zero biases of the equivalent FOGs and the DFOG are shown in Fig. 4. And their Allan variances are plotted

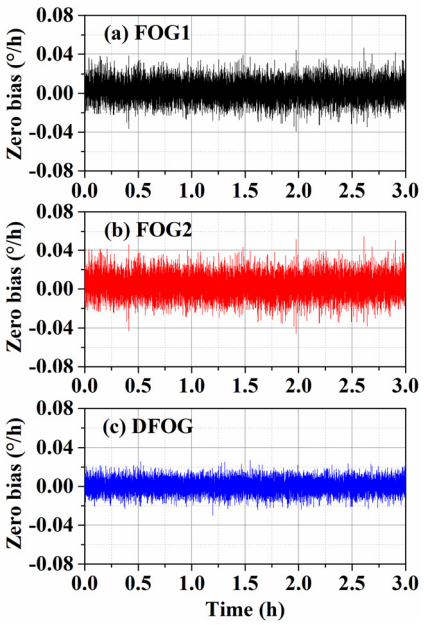

FIGURE 4. Bias test results of the two equivalent FOGs and DFOG (1s sampling rate).

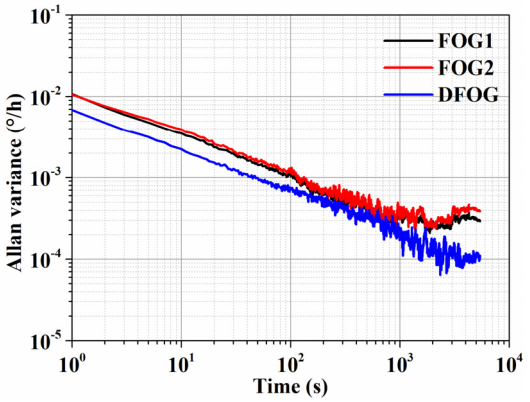

FIGURE 5. Allan variance curves of the equivalent FOGs and DFOG.

in Fig. 5. The bias drift (100s integration, 1σ) of FOG1, FOG2 and DFOG are 1.05×10^{-3}°/h, 1.17×10^{-3}°/h, and 7.07×10^{-4}°/h respectively. And their values of ARW are 1.61×10^{-4} °/h$^{1/2}$, 1.93×10^{-4}°/h$^{1/2}$ and 1.32×10^{-4} °/h$^{1/2}$ respectively.

As shown in Fig. 5, the profiles of Allan variance curves of FOG1 and FOG2 are similar and show obvious Allan deviation due to rate random walk (RRW) and rate ramp [18] which are closely related to the polarization non-reciprocity, coherent back reflection, backscatter noises, and, time transience-related nonreciprocal effects, etc. in the SIA. And there are no obvious RRW and rate ramp features on the Allan deviation curve of DFOG after the differential processing. This proves the former noise can be reduced effectively by use of differential processing. Based on the characteristic of RIN [18], the random noise associated with may be reduced too because the equivalent operational bandwidth becomes wider in DFOG when the two broadband SLDs

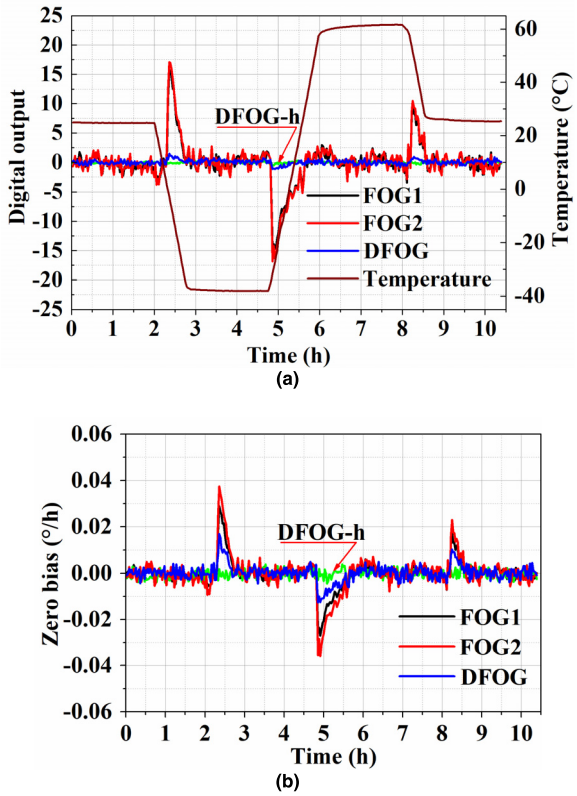

FIGURE 6. Results of bias drift measurement under transient temperature (100s integration). (a) Digital outputs of the equivalent FOGs and DFOG, (b) The corresponding zero biases. The brown curve is the applied transient temperature. The black, red and blue curves correspond to FOG1, FOG2, and DFOG. The green curve is the compensated curve (marked as DFOG-h) by introducing the compensation factor *h* so that the drift due to "Shupe" effect is almost eliminated.

are equivalent to an ultra-wide spectral light source [17]. Therefore, although the scale factor of DFOG is smaller than that of the equivalent FOGs, the bias drift and ARW are both reduced effectively and considerably smaller than that of individual FOGs.

IV. THE EFFECT OF TEMPERATURE TRANSIENCE

The bias drifts of the equivalent FOGs and DFOG were tested when subjected to transient temperature variation. The SIA was packaged in a cylindrical aluminum box and mounted in a temperature chamber on a rotation stage, the rest of the DFOG was placed outside the temperature chamber. The temperature of the SIA was monitored by a Pt thermometer. The experimental temperature was varied from −40 to +60° C and the running steps were as follows: (25°C, 120mins), (25°C to −40°C, 43mins), (−40°C, 120mins), (−40°C to 60°C, 67mins), (60°C, 120mins), (60°C to 25°C, 23mins) and (25°C, 120mins). At the rise and fall edge, the speed of temperature variation was about 1.5 °C/min. The experiment ran about 10.5 hrs. The digital outputs of the two equivalent FOGs, the DFOG and the values of temperature were recorded with 1s sampling rate synchronously. After being subtracted the local component of earth rotation, the experimental results (100s integration) are shown in Fig. 6.

Figure 6(a) shows the temperature applied to the DFOG, as well as the measured digital outputs of the equivalent FOGs and DFOG, while Figure 6(b) shows the corresponding zero biases in terms of rotation rate. It can be seen that the zero biases of FOG1 (black) and FOG2 (red) show typical profiles of drift due to "Shupe" effect, while the zero bias (blue) of DFOG is considerably smaller. The values of the bias drift (1σ, 100s) are 6.17×10^{-3}°/h, 7.76×10^{-3}°/h and 4.09×10^{-3}°/h for FOG1, FOG2 and DFOG over the test period of 10.5 hours. These preliminary experimental results indicate that the bias drift due to temperature transience are reduced with the DFOG.

As shown in Fig. 6(b), there is obvious residual drift (blue) in the zero-bias curve of DFOG because the dispersion of PM fiber used for the fiber coil is weak and the value of D_1/λ_1 is far from that of D_2/λ_2. From (8), we can predict that the residue bias drift of the DFOG could be completely eliminated by multiplying the output of one of the equivalent FOGs with a dispersion compensation factor h, before taking the differential processing. Then, equations (4), (8) and K_{SD} may be rewritten as:

$$v_D = v_1 - h \cdot v_2 = K_1\varphi_1 - h \cdot K_2\varphi_2 = K_D \cdot (\varphi_1 - h \cdot \varphi_2), \tag{10}$$

$$\Delta\varphi_e = F \cdot (\frac{D_1}{\lambda_1} - h \cdot \frac{D_2}{\lambda_2}), \tag{11}$$

$$K_{SD} = \frac{2\pi LD}{c} \cdot \frac{\lambda_2 - h\lambda_1}{\lambda_1\lambda_2}. \tag{12}$$

Obviously, the use of dispersion compensation factor affects the scale factor of the DFOG. From (10), we may get the value of h by using the digital outputs of FOG1 and FOG2 (shown in Fig. 6 (a)) to minimize v_D. By the least squares fitting method, the optimal value of h is found to be 0.933. And the K_{SD} and SF_D of DFOG are re-calibrated and become 432452 $(°/s)^{-1}$ and 1.80069 s, respectively. The compensated results of the DFOG are also shown in Fig. 6 as the green curve and marked as DFOG-h. After inducing the h factor, we can see that the bias drift (100s integration, 1σ) of DFOG under temperature transience becomes 1.52 $\times 10^{-3}$°/h, which is ∼2.7 times smaller than the uncompensated DFOG, indicating that the drift due to "Shupe" effect is significantly reduced.

Form (11), the value of h to minimize error due to Shupe effect may be expressed as:

$$h = \frac{D_1}{D_2} \cdot \frac{\lambda_2}{\lambda_1}. \tag{13}$$

When the wavelengths of the two SLDs are selected, the value of h will be determined by the ratio of dispersion coefficient D_1 and D_2, as defined by (7). For the DFOG used in our experiments, the PM fiber coil was fabricated by the symmetrical quadrupolar winding method and the UV glue was used to fill the gap between fibers during the winding process, cured and heat-treated specially in the end. This polymer coating could change the actual index dependence dn_{cj}/dT as well as the actual thermal expansion coefficient α of the complex composite structure of the coil composed of silica fiber,

which may cause nonuniform temperature-induced stresses and induce much larger dispersion coefficient of dn_{cj}/dT in the coil [19], [20].

With the method reported in [21], we measured roughly the values of the actual effective refractive index and dn_{cj}/dT of the PM fiber used for the coil along its operational slow axis at wavelengths of 1310 and 1550 nm. The measured values are 1.4663 and 9.81×10^{-6} /°C at 1300 nm, 1.4685 and 12.38×10^{-6} /°C at 1550 nm respectively. Compared with the results in [21], [22], the measured value of dispersion and dn_{cj}/dT become obviously larger, but the tendency of variation is the same. The results are consistent with the above discussion. Because the second term αn_{cj} in the expression equation of D_j in (7) is relatively smaller, the value of h may be estimated from the contribution of dn_{cj}/dT alone. Based on the measured parameters and the wavelengths listed in Table 1, the value of h is calculated to be ~ 0.946 and close to the one obtained from fitting the experimental result. Based on the above discussion and the experimental results, we can conclude that the dispersion compensation factor h is closely related to the PM fiber, glue and winding/curing process during the fabrication of the PM fiber coil. After a long time of heat treatment, the overall properties of the fiber coil, including dispersion, will stabilize and the reliable and accurate value of h can be obtained based on the above experiment and fitting method and it is a reasonable way to obtain dispersion coefficient by fitting to the experimental results.

V. CONCLUSION

In conclusion, a novel DFOG driven by two broadband sources is proposed and experimentally demonstrated. In the DFOG, two equivalent FOGs operate separately with two sources of different wavelengths and share one Sagnac interferometer assembly. Comparing with the individual FOGs, the DFOG achieves better bias drift as well as angle random walk, due to the good common-mode error rejection capability of the system. In particular, the bias drift of the DFOG due to temperature transience could be largely reduced or even eliminated by introducing a dispersion compensation factor h in the differential operation. However, it operates in open loop mode now and has a limited measure range. The DFOG is a potential candidate for the platform inertial system and geographical rotation measure system to achieve high performance without using sophisticated precision temperature control.

REFERENCES

[1] Y. N. Korkishko, V. A. Fedorov, V. E. Prilutskiy, V. G. Ponomarev, I. V. Fedorov, S. M. Kostritskii, I. V. Morev, D. V. Obuhovich, S. V. Prilutskiy, A. I. Zuev, and V. K. Varnakov, "Highest bias stability fiber-optic gyroscope SRS-5000," in *Proc. DGON Inertial Sensors Syst. (ISS)*, Karlsruhe, Germany, Sep. 2017, pp. 1–23.

[2] G. A. Sanders, S. J. Sanders, L. K. Strandjord, T. Qiu, J. Wu, M. Smiciklas, D. Mead, S. Mosor, A. Arrizon, W. Ho, and M. Salit, "Fiber optic gyro development at Honeywell," *Proc. SPIE*, vol. 9852, May 2016, Art. no. 985207.

[3] H. C. Lefèvre, "Potpourri of comments about the fiber-optic gyro for its 40th anniversary, and how fascinating it was and it still is," *Proc. SPIE*, vol. 9852, May 2016, Art. no. 985203.

[4] H. C. Lefèvre, "The fiber-optic gyroscope: Challenges to become the ultimate rotation-sensing technology," *Opt. Fiber Technol.*, vol. 19, no. 6, pp. 828–832, Dec. 2013.

[5] K. Iwatsuki, "Excess noise reduction in fiber gyroscope using broader spectrum linewidth er-doped superfluorescent fiber laser," *IEEE Photon. Technol. Lett.*, vol. 3, no. 3, pp. 281–283, Mar. 1991.

[6] K. Killian, M. Burmenko, and W. Hollinger, "High performance fiber optic gyroscope with noise reduction," *Proc. SPIE*, vol. 2292, pp. 255–263, Nov. 1994.

[7] F. Guattari, S. Chouvin, C. Molucon, and H. Lefevre, "A simple optical technique to compensate for excess RIN in a fiber-optic gyroscope," in *Proc. DGON Inertial Sensors Syst. (ISS)*, Karlsruhe, Germany, Sep. 2014, pp. 1–4.

[8] J. Honthaas, J. Bonnefois, E. Ducloux, and H. Lefèvre, "Interferometric filtering of the excess relative intensity noise of the broadband source of a fiber optic gyroscope," *Proc. SPIE*, vol. 9157, Jun. 2014, Art. no. 91572D.

[9] C. Zhang, Y. Mao, X. Zhou, and G. Ren, "Application of the Wiener filter for intensity noise reduction in fiber optic gyroscopes," *Appl. Opt.*, vol. 58, no. 20, p. 5568, Jul. 2019.

[10] D. M. Shupe, "Thermally induced nonreciprocity in the fiber-optic interferometer," *Appl. Opt.*, vol. 19, no. 5, p. 654, Mar. 1980.

[11] R. Luo, Y. Li, S. Deng, D. He, C. Peng, and Z. Li, "Compensation of thermal strain induced polarization nonreciprocity in dual-polarization fiber optic gyroscope," *Opt. Express*, vol. 25, no. 22, p. 26747, Oct. 2017.

[12] N. J. Frigo, "Compensation of linear sources of non-reciprocity in Sagnac interferometers," *Proc. SPIE*, vol. 0412, pp. 268–271, Sep. 1983.

[13] W. Ling, X. Li, Z. Xu, Z. Zhang, and Y. Wei, "Thermal effects of fiber sensing coils in different winding pattern considering both thermal gradient and thermal stress," *Opt. Commun.*, vol. 356, pp. 290–295, Dec. 2015.

[14] H. Yang, L. Qiao, Y. Yang, W. Huang, and S. Sun, "Thermally induced error analysis and suppression of optic fiber delay loop in the different variable rate of temperature," *Optik*, vol. 193, Sep. 2019, Art. no. 162994.

[15] P. Lu, Z. Wang, R. Luo, D. Zhao, C. Peng, and Z. Li, "Polarization nonreciprocity suppression of dual-polarization fiber-optic gyroscope under temperature variation," *Opt. Lett.*, vol. 40, no. 8, p. 1826, Apr. 2015.

[16] G. Wang, Q. Wang, B. Zhao, and Z. Wang, "Compensation method for temperature error of fiber optical gyroscope based on relevance vector machine," *Appl. Opt.*, vol. 55, no. 5, p. 1061, Feb. 2016.

[17] Y. Yang, S. Li, H. Yan, and W. Jin, "Low-noise closed-loop FOG driven by two broadband sources," *J. Lightw. Technol.*, vol. 37, no. 18, pp. 4555–4559, Sep. 15, 2019.

[18] H. C. Lefèvre, *The Fiber-Optic Gyroscope*, 2nd ed. Boston, MA, USA: Artech House, 2014, pp. 62–63, 50, and 203, 2014.

[19] H. Mueller, "The theory of photoelasticity," *J. Amer. Ceram. Soc.*, vol. 21, no. 1, pp. 27–33, Jan. 1938.

[20] A. H. Hartog, A. J. Conduit, and D. N. Payne, "Variation of pulse delay with stress and temperature in jacketed and unjacketed optical fibres," *Opt. Quantum Electron.*, vol. 11, no. 3, pp. 265–273, May 1979.

[21] J. J. Carr, S. L. Saikkonen, and D. H. Williams, "Refractive index measurements on single-mode fiber as functions of product parameters, tensile stress, and temperature," *Fiber Integr. Opt.*, vol. 9, no. 4, pp. 393–396, Oct. 1990.

[22] L. Yuan, "Effect of temperature and strain on fiber optic refractive index," *Acta Optica Sinica*, vol. 17, no. 12, pp. 1713–1717, Dec. 1997.

YUANHONG YANG received the Ph.D. degree from Beihang University, Beijing, China, in 2004. He is currently a Professor and a Ph.D. Supervisor with the School of Instrumentation and Optoelectronic Engineering, Beihang University. His research interests include fiber optic gyroscope, photoelectron devices, and distributed optical fiber sensing technology.

SHUAI LI received the B.S. degree from Harbin Engineering University, China, in 2016. He is currently pursuing the Ph.D. degree with the School of Instrumentation and Optoelectronic Engineering, Beihang University. His research interests include fiber optic gyroscope and optical fiber sensing technology.

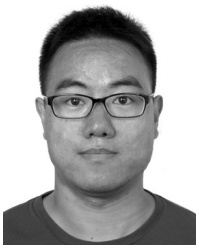

FULING YANG received the B.S. and M.S. degrees from the Harbin Institute of Technology, China, in 2011 and 2013, respectively, and the Ph.D. degree from Beihang University, China, in 2018. He is currently a Lecturer with the School of Mechanical Electronic and Information Engineering, China University of Mining and Technology, Beijing. His research interests include fiber optic gyroscope, fiber optic gas sensing technology, and fiber grating sensing technology.

WEI JIN received the Ph.D. degree in optical fiber from Strathclyde University, U.K., in 1991. He is currently a Professor with the Department of Electrical Engineering, The Hong Kong Polytechnic University. His research interests include fiber sensing, photonic crystal fiber theory, fiber gas sensing technology, and fiber grating sensing technology.